Energy Harvesting from Crystalline and Conductive Polymer Composites

Aravind Kumar, Shaikh Faruque Ali and A. Arockiarajan

Abstract Modern electronic devices require less energy on-board and could be powered by energy harvested from the environment. Mechanical vibrations are attractive sources for energy harvesting due to their high availability in technical environments. Among the various mechanisms available to convert mechanical energy into electrical energy, piezoelectric transduction offers high power density at microenergy scales. In piezoelectric energy harvesters, the amount of electrical energy harvested directly depends on the strain undergone by the transducer. Commonly used piezoelectric transducers are made of perovskite ceramics such as PZT and are brittle. This limits the maximum allowable strain in the harvester and consequently the power harvested. In such cases, electroactive polymers act as viable alternatives due to their flexibility. Energy harvesting from conductive and crystalline electroactive polymers is explored in this chapter. Crystalline polymers such as polyurethane and semicrystalline polymers such as PVDF are commonly used in energy harvesting devices owing to their flexibility, affordability, and good electromechanical coupling properties. This chapter begins with a brief account on the material properties of PVDF and polyurethane. Subsequently, design of energy harvesters based on these materials is elucidated. A short note on energy harvesting from crystalline biopolymers such as cellulose nanocrystals is also included therein. Such harvesters are attractive as they are environment friendly and biocompatible. Among conductive polymer composites, harvesters based on polyaniline and carbon nanotubes are described. A comparison between the harvesting capabilities of different electroactive polymers and the challenges faced are discussed to draw an overall picture on energy harvesting from electroactive polymers.

Keywords Energy harvesting · Electroactive polymers · PVDF · Cellulose nanocrystals · Piezoelectricity · Polyurethane · Electrostriction · Conducting polymers · Thermogalvanic cells · Carbon nanotubes

A. Kumar · S.F. Ali (✉) · A. Arockiarajan
Department of Applied Mechanics, Indian Institute of Technology Madras, Chennai 600036, India
e-mail: sfali@iitm.ac.in

D. Ponnamma et al. (eds.), *Smart Polymer Nanocomposites*,
Springer Series on Polymer and Composite Materials,
DOI 10.1007/978-3-319-50424-7_2

Contents

1 Introduction 44
2 Electroactive Polymers (EAPs) 45
3 Energy Harvesting from Ferroelectric Polymers 47
3.1 Electromechanical Properties of PVDF 48
3.2 Energy Harvesting Using PVDF 52
3.3 Energy Harvesting Using Cellulose Nanocrystals 59
4 Energy Harvesting from Electrostrictive Polymers 61
4.1 Effect of Intrinsic Mechanisms 62
4.2 Tackling Quadratic Dependence of Strain on Electric Field 63
4.3 Energy Harvesting Using Polyurethane Transducers 64
5 Comparison of Electromechanical Coupling in Various Dielectric EAPs 68
6 Energy Harvesting from Conductive Polymer Composites 69
6.1 Thermoelectric Energy Harvesters with Carbon Nanotube Electrodes 70
7 Summary 72
References 73

1 Introduction

The realm of wireless devices is witnessing an exponential growth ever since its inception. But the extent of services offered by these devices is often limited by the lifetime of batteries powering them. A self-sustainable power source would thus thrust us forward to exploit the potential of such devices exhaustively. The current technological revolution is propelled by miniaturization, and as devices continue to shrink, less energy is required on-board. This has encouraged the researchers to explore the possibility of augmenting batteries with systems that continuously scavenge otherwise wasted energy from the environment [1–3]. This process of converting otherwise wasted ambient energy into a useful form is called *energy harvesting or scavenging*.

Energy harvesting would augment sustainable power supply to a wireless system network and might even offset the need to replace and to maintain the batteries in areas that are either inhospitable or difficult to reach. This includes applications such as safety monitoring devices, structure-embedded microsensors, and medical implants, to name a few. There are also environmental benefits associated with energy harvesting as it provides a 'battery-less' solution by scavenging energy from ambient energy sources such as vibrations, heat, light, and water and converting it into electrical power [4].

Mechanical energy harvesting converts energy from movement or vibration into electrical energy. The mechanical energy sources encompass vibrations and noise from industrial machinery and equipment, transportation, fluid flow such as air movements, biological locomotion such as walking, or in-body motion such as chest and heart movement. In general, there are two main ways of extracting energy from a mechanical source, *inertial* and *kinematic* [5].

Inertial energy harvesting relies on the resistance to acceleration of a mass. These systems consist of a spring-mass-damper system connected to the base at a single point. When the base moves, the mass vibrates due to its inertia, and these vibrations can be converted into electrical energy. Examples of harvester designs exploiting this principle of inertia include those based on cantilever beams [6, 7], pendulums [8, 9], and magnetoelastic oscillators [10–12].

In kinematic energy harvesting, the energy harvesting transducer is directly coupled to different parts of the source. The relative motion between these parts leads to a deformation in the transducer, which is then converted into electrical energy. Examples include harvesting energy from the bending of a tire wall to monitor pressure, or the flexing and extension of limbs to power mobile.

At present, mechanical-to-electricity energy conversion is mostly accomplished via electrostatic, electromagnetic, or piezoelectric transduction mechanisms [13]. Power density for piezoelectric transduction exceeds that for electromagnetic generators below 0.5 cm^3 [14], and consequently, they represent promising materials for electromechanical energy conversion technologies at smaller scales.

In piezoelectric energy harvesting, the power harvested is directly dependent on the strain and the electromechanical coupling coefficient of the material employed for electromechanical transduction. Piezoelectric ceramics such as lead zirconate titanate and barium titanate have very high electromechanical coupling coefficients, but they are very brittle, with the maximum strain that they can undergo being limited to 0.2% in case of polycrystalline materials and 1% in case of single-crystal piezoelectrics [15]. On the other hand, electroactive polymers (EAPs) generally undergo strains greater than 1%, and certain classes of EAPs can even go up to 50% [15]. But the electromechanical coefficient of EAPs is comparatively less than that of piezoceramics. Hence, in either case, the limitation of the material sets an upper bound to the power that can be harvested from the motion of the host structure. Hence, current research focuses on improving the ductility of piezoceramics and the coupling coefficient of electroactive polymers.

Knowledge of existing energy harvesting technologies, their advantages, and limitations would be essential in setting up the foundation for future research directions in the field. Hence, this chapter is dedicated to such a comprehensive review on energy harvesting technologies, particularly involving conductive and crystalline electroactive polymers. The properties of various electroactive polymers will be discussed initially, and further discussions will focus on the design and analysis of energy harvesters based on these polymers.

2 Electroactive Polymers (EAPs)

EAPs are polymers that undergo a change in shape and dimensions when subjected to an electric field [16]. EAPs are primarily used as actuators in aerospace [17–19], medical [20], and robotics [21] applications. They are also used as artificial muscles

in biomimetic applications [16, 22]. Recently, researchers have started to explore the power scavenging capabilities of EAPs. Most of the EAPs get electrically polarized when subjected to a mechanical strain. Since EAPs are flexible and can undergo large deformations, they are seen as potential alternatives for the conventional piezoceramics in the field of energy harvesting.

EAPs are classified into two families, namely electronic and ionic [16]. Electronic EAPs exhibit electromechanical coupling due to polarization based or electrostatic mechanisms [15]. Electronic EAPs are insulators and contain bound charges in the form of electric dipoles. Most of the electronic EAPs are either crystalline or semicrystalline. The crystal units within these polymers contain atoms with partial charges and generate dipole moments. For example, the electromechanical coupling in polyvinylidene fluoride (PVDF) is provided by a polar crystalline phase resulting from the spatially symmetric location of fluorine and hydrogen atoms along the polymer chain [23]. Thus, the inherent electromechanical coupling in polymers such as PVDF can be attributed to their crystalline nature. However, there are few amorphous polymers which exhibit electromechanical coupling. In such polymers, the electromechanical coupling is due to the freezing of electrical dipoles in the material below the glass transition temperature [23]. Examples of this type include polyimides.

Based on the relation between mechanical strain and electric polarization, the electronic EAPs can be further divided into ferroelectric and electrostrictive. Ferroelectric polymers exhibit a linear relationship between strain and polarization, whereas in electrostrictive polymers, strain is proportional to the square of polarization. PVDF is a classic example of ferroelectric polymer, while its co-polymers with trifluoroethylene (P(VDF-TrFE)) are electrostrictive. Another electrostrictive polymer, polyurethane, is also widely used for energy harvesting.

Ionic EAPs exhibit electromechanical coupling due to the diffusion of charged species within the polymer network. The diffusion of charged molecules or atoms gives rise to electrical conductivity in ionic EAPs. Such diffusion also leads to electromechanical coupling in these materials due to the accumulation of charges within the material [15].

Ionic EAPs are further subdivided into ionic polymer–metal composites (IPMCs) and conductive polymer composites [24]. IPMCs are based on ionic migration through a selective ionic membrane. Such selective ionic membranes allow only a particular species of ions (either anions or cations) to pass through them. Examples of this kind include Nafion and Flemion. Nafion is used in selective migration of hydrogen ions in proton exchange membrane fuel cells (PEMFCs). Conductive polymer composites undergo redox reactions in the presence of an electrolyte and, consequently, exhibit a change in volume. Polyaniline and polypyrrole are examples of this type. Electrical energy can be harvested from a conductive polymer composite kept in an electrolyte medium through the mechano-chemo-electric process, but the efficiency is very low [25]. However, composites made of conducting fillers such as carbon nanotubes and polymer materials such as PVDF and polydimethylsiloxane (PDMS) have better electromechanical coupling and are widely used in energy harvesting.

The energy harvesters based on ferroelectric, electrostrictive, and conductive polymers differ in their working principle. The material behavior plays an important role in the harvester design. Hence, a brief introduction to the properties of these materials is given, and energy harvesters based on these materials are discussed subsequently. Among crystalline polymers, the harvesters based on PVDF (ferroelectric semicrystalline polymer), cellulose nanocrystals (piezoelectric biopolymer), and polyurethane (electrostrictive polymer) are elucidated. Among polymers, harvesting energy using polyaniline, polypyrrole, and conducting polymer composites with carbon nanotube fillers is described to illustrate the principles involved.

3 Energy Harvesting from Ferroelectric Polymers

Ferroelectric materials are those which exhibit, at temperatures below Curie temperature (T_c), a domain structure and spontaneous polarization which can be reoriented by applied electric fields [23]. Common examples of ferroelectric materials are the perovskite ceramics such as barium titanate ($BaTiO_3$) and lead zirconate titanate (PZT) and polymers such as PVDF.

The domain morphology of ferroelectric materials results from the alignment of dipoles to minimize electrostatic and elastic energy, and materials with this structure will exhibit varying degrees of hysteresis at all drive levels. In the unpoled state (paraelectric phase), a positive strain is realized in these materials, whatever be the direction of application of electric field. To achieve bidirectional strains, these materials are poled and operated around this poled state. For low-to-moderate input fields, the response of the material around this poled state is approximately linear. Such materials operating in these linear regimes are designated as piezoelectric materials [23]. However, the terms ferroelectricity and piezoelectricity are interchangeably used in many literature, and this is a common misnomer.

Piezoelectricity is observed in a variety of synthetic polymers such as polypropylene, polystyrene, and nylon-11. Biopolymer substances such as cellulose with an asymmetric crystal structure also exhibit piezoelectricity. But the electromechanical coupling in these materials is very weak. Strong electromechanical coupling has been observed only in PVDF and its co-polymers. The piezoelectric properties of PVDF were discovered by Kawaii in 1969. PVDF is a semicrystalline polymer with approximately 50% crystallinity [26]. The molecular structure of PVDF consists of the repeated monomer unit **–CF_2–CH_2–**. The atoms are covalently bonded, forming long molecular chains. The hydrogen atoms are positively charged, and the fluorine atoms are negatively charged with respect to the carbon atoms, giving rise to electric dipoles within individual crystallites. Hence, PVDF is inherently polar. However, the average macroscopic polarization of the unpoled material is zero due to the random orientation of the individual crystallites. Permanent dipole polarization of PVDF is generally obtained by stretching and

polarizing extruded thin sheets of the polymer. A review of the various polarization methods is given by Sessler [27].

Typically, PVDF is produced in thin films whose thicknesses range from 9 to 800 μm (10^{-6} m). A thin layer of nickel, silver, or copper is deposited on both surfaces to provide electrical conductivity when an electric field is applied, or to allow measuring the charge induced by mechanical deformation [26].

3.1 Electromechanical Properties of PVDF

Typically, the piezoelectric properties of PVDF are determined within the framework of linear piezoelectric theory. The basic properties of a piezoelectric material are expressed mathematically as a relationship between two mechanical variables, stress σ and strain ε, and two electrical variables, electric field E and electric displacement D. Generally, applying stress to an elastic material will result in the deformation of the material. The ratio of change in dimension to the original dimension is called the strain. Assuming a uniaxial state of strain, the stress σ and strain ε along the direction of loading can be related by the Hooke's law:

$$\varepsilon = \frac{1}{Y}\sigma = S\sigma \tag{1}$$

where Y is the modulus of elasticity of the material and $S = 1/Y$ is the inverse of the modulus of elasticity known as compliance of the material.

For a piezoelectric material, the application of a mechanical stress also leads to accumulation of surface charges in the material, in addition to the mechanical strain. This is known as the direct piezoelectric effect. The surface charge accumulated per unit area is defined as the electric displacement D and is related to the stress as follows:

$$D = d\sigma \tag{2}$$

where d is known as the piezoelectric strain coefficient and is a measure of the coupling between mechanical and electrical domains. The piezoelectric strain coefficient d is equal to the eigenstrain developed in the piezoelectric material on application of unit electric field to the material. This definition is derived from the inverse piezoelectric effect which is elucidated by Eq. (3).

Just as the application of mechanical stress leads to an electric displacement, the application of an electric field also produces a mechanical strain in a piezoelectric material. This converse phenomenon is known as the inverse piezoelectric effect. The electric field and strain are related by:

$$\varepsilon = dE \tag{3}$$

All piezoelectric materials act as electrical insulators (dielectrics) and hence become polarized under the influence of an external electric field. The resulting electric displacement can be related to the applied electric field as follows:

$$D = \kappa E \tag{4}$$

Equations (1) to (4) can be combined together to give the linear constitutive relations for piezoelectric materials:

$$\varepsilon = S\sigma + dE \tag{5}$$

$$D = \kappa E + d\sigma \tag{6}$$

Equations (5) and (6) give the piezoelectric constitutive law with stress σ and electric field E as independent variables. The law can also be expressed by taking the fields (σ, D), (ε, D), and (ε, E) as independent variables to suit the modeling requirements. For a detailed discussion on the appropriate transformations that aid the conversion between one form and the other, please refer [15].

The piezoelectric constitutive relations can be extended to fit in a general three-dimensional scenario as follows:

$$\varepsilon_{ij} = s_{ijkl}\sigma_{kl} + d_{ijn}E_n \tag{7}$$

$$D_n = \kappa_{nm}E_m + d_{nij}\sigma_{ij} \tag{8}$$

The quantities stress σ and strain ε are second-order tensors, while electric field E and electric displacement D are first-order tensors. Mechanical compliance S is a fourth-order tensor, dielectric permittivity κ is a second-order tensor, and piezoelectric strain coefficient d is a third-order tensor.

Rewriting the above in Voigt notation, we obtained the following:

$$\begin{Bmatrix} \varepsilon_1 \\ \varepsilon_2 \\ \varepsilon_3 \\ \varepsilon_4 \\ \varepsilon_5 \\ \varepsilon_6 \\ D_1 \\ D_2 \\ D_3 \end{Bmatrix} = \begin{bmatrix} S_{11} & S_{12} & S_{13} & S_{14} & S_{15} & S_{16} & d_{11} & d_{21} & d_{31} \\ S_{12} & S_{22} & S_{23} & S_{24} & S_{25} & S_{26} & d_{12} & d_{22} & d_{32} \\ S_{13} & S_{23} & S_{33} & S_{34} & S_{35} & S_{36} & d_{13} & d_{23} & d_{33} \\ S_{14} & S_{24} & S_{34} & S_{44} & S_{45} & S_{46} & d_{14} & d_{24} & d_{34} \\ S_{15} & S_{25} & S_{35} & S_{45} & S_{55} & S_{56} & d_{15} & d_{25} & d_{35} \\ S_{16} & S_{26} & S_{36} & S_{46} & S_{56} & S_{66} & d_{16} & d_{26} & d_{36} \\ d_{11} & d_{12} & d_{13} & d_{14} & d_{15} & d_{16} & \kappa_{11} & \kappa_{12} & \kappa_{13} \\ d_{21} & d_{22} & d_{23} & d_{24} & d_{25} & d_{26} & \kappa_{12} & \kappa_{22} & \kappa_{23} \\ d_{31} & d_{32} & d_{33} & d_{34} & d_{35} & d_{36} & \kappa_{13} & \kappa_{23} & \kappa_{33} \end{bmatrix} \begin{Bmatrix} \sigma_1 \\ \sigma_2 \\ \sigma_3 \\ \sigma_4 \\ \sigma_5 \\ \sigma_6 \\ E_1 \\ E_2 \\ E_3 \end{Bmatrix} \tag{9}$$

where the subscripts 1, 2, and 3 denote the normal components and 4, 5, and 6 denote the shear components, respectively.

Most of the piezoelectric materials are transversely isotropic; hence, the compliance matrix will only have five independent constants as opposed to 21 as in Eq. (9). The electric field applied in a particular direction will not produce electrical displacements along orthogonal directions. Hence, the dielectric permittivity matrix will reduce to a diagonal matrix. Due to transverse isotropy, the dielectric permittivity along directions 1 and 2 will be equal, and hence, the dielectric permittivity matrix will have only two independent constants. Piezoelectric materials, when poled, exhibit cubic symmetry. If the poling is assumed to be along the 3-direction, then cubic symmetry implies that all the coefficients other than d_{31}, d_{32} d_{33}, d_{15}, and d_{24} vanish to zero [15]. Transverse isotropy leads to a further reduction in the piezoelectric strain matrix with $d_{31} = d_{32}$, $d_{15} = d_{24}$. Hence, the piezoelectric strain matrix will have only three independent constants. Reflecting all these changes in the material properties, Eq. (9) will reduce to:

$$\begin{Bmatrix} \varepsilon_1 \\ \varepsilon_2 \\ \varepsilon_3 \\ \varepsilon_4 \\ \varepsilon_5 \\ \varepsilon_6 \\ D_1 \\ D_2 \\ D_3 \end{Bmatrix} = \left[\begin{array}{cccccc:ccc} S_{11} & S_{12} & S_{11} & 0 & 0 & 0 & 0 & 0 & d_{31} \\ S_{12} & S_{11} & S_{13} & 0 & 0 & 0 & 0 & 0 & d_{31} \\ S_{13} & S_{13} & S_{33} & 0 & 0 & 0 & 0 & 0 & d_{33} \\ 0 & 0 & 0 & S_{44} & 0 & 0 & 0 & d_{15} & 0 \\ 0 & 0 & 0 & 0 & S_{55} & 0 & d_{15} & 0 & 0 \\ 0 & 0 & 0 & 0 & 0 & 2(S_{11}-S_{12}) & 0 & 0 & 0 \\ \hdashline 0 & 0 & 0 & 0 & d_{15} & 0 & \kappa_{11} & 0 & 0 \\ 0 & 0 & 0 & d_{15} & 0 & 0 & 0 & \kappa_{11} & 0 \\ d_{31} & d_{31} & d_{33} & 0 & 0 & 0 & 0 & 0 & \kappa_{33} \end{array}\right] \begin{Bmatrix} \sigma_1 \\ \sigma_2 \\ \sigma_3 \\ \sigma_4 \\ \sigma_5 \\ \sigma_6 \\ E_1 \\ E_2 \\ E_3 \end{Bmatrix} \tag{10}$$

The elastic, electrical, and piezoelectric properties of PVDF and the most commonly used piezoelectric ceramic PZT are compared in Table 1. From Table 1, it is observed that the piezoelectric strain coefficient d is comparatively small for PVDF than PZT. This implies that for the same external electric field applied, PZT would produce more strain than PVDF. This is concerned with the actuation capabilities of the two materials. However, we are interested in exploring the energy harvesting potential of the materials. To do so, we look at the piezoelectric stress coefficient g of the two materials. The piezoelectric stress coefficient g is a measure

Table 1 Elastic, dielectric, and piezoelectric properties of PVDF and PZT

Property	Symbol	PVDF	PZT-5A
Modulus of elasticity (N/mm^2)	Y	2×10^9	7.4×10^{10}
Poisson's ratio	v	0.34	0.35
Relative dielectric permittivity	κ_r	12	1800
Piezoelectric strain coefficient (pC/N)	d_{31}	22	−175
	d_{33}	−30	450
Piezoelectric stress coefficient (Vm/N)	g_{31}	0.216	−0.011
	g_{33}	−0.33	0.027
Piezoelectric coupling coefficient	k_{31}	0.14	0.34

of voltage developed per unit length of the material under the influence of an external mechanical stress. From Table 1, we see that the piezoelectric stress coefficient is about 10 times higher for PVDF than PZT. Hence, PVDF is an excellent candidate for energy harvesting applications and will provide higher voltage output than PZT for the same amount of mechanical stress applied. But, the elastic modulus of PVDF is very low compared to that of PZT, which means that PVDF will be subjected to a lower mechanical stress compared to that of PZT for the same amount of strain applied.

From the above argument, it is evident that the electromechanical conversion efficiency depends not only on the piezoelectric strain or stress coefficients but also on modulus of elasticity and dielectric permittivity. It would be helpful to express a quantity that takes into account the effect of all these material properties on electromechanical energy conversion. One such quantity is the piezoelectric coupling coefficient which is defined as [15],

$$k_{ij} = \frac{d_{ij}}{\sqrt{k_{ii}^{\sigma} S_{jj}^{E}}} \tag{11}$$

where the subscripts i and j indicate the components as in Voigt notation, and the superscripts σ and E denote that the properties are measured at constant stress and electric fields, respectively.

The piezoelectric coupling coefficient is related to the electromechanical conversion efficiency such that [24]:

$$k_{ij}^2 = \frac{\text{tranformed energy}}{\text{input energy}} \tag{12}$$

Hence, higher the coupling coefficient, higher the mechanical energy converted into electrical energy and vice versa.

For the commonly used 33- and 31-modes of transduction, the coupling coefficient can be defined as follows:

$$k_{33} = \frac{d_{33}}{\sqrt{\kappa_{33}^{\sigma} S_{33}^{\mathrm{E}}}} \tag{13}$$

$$k_{31} = \frac{d_{31}}{\sqrt{k_{33}^{\sigma} S_{11}^{\mathrm{E}}}} \tag{14}$$

The 31-mode coupling coefficients of PZT and PVDF are also shown in Table 1. Higher values of coupling coefficient for PZT show that it is more efficient than PVDF. Nevertheless, both the materials are extensively used in energy harvesting applications, as the ductility of PVDF provides an edge over PZT in certain cases.

3.2 *Energy Harvesting Using PVDF*

PVDF has a high piezoelectric strain coefficient compared to that of other polymers, and consequently, it is a suitable candidate for energy harvesting applications. The flexibility and the maneuverability of PVDF to form complex shapes augments the same. PVDF transducers can withstand high strains than their PZT counterparts. This justifies the use of PVDF in kinematic energy harvesters. Kinetic energy harvesters make use of both PZT and PVDF as transducer materials. The design of both kinematic and kinetic energy harvesters employing PVDF transducers is elucidated next.

3.2.1 Kinetic Energy Harvesters Using PVDF

In kinetic piezoelectric energy harvesters, the vibrations setup in a spring-mass-damper system is used to strain the piezoelectric material. One of the most common ways of achieving this is to connect a spring-mass-damper system to a vibrating source at a point. The mass oscillates due to excitation from the source. The kinetic energy from the oscillations is converted into electrical energy with the help of piezoelectric transducers.

As mentioned earlier, piezoelectric transducers used for commercial applications are generally poled. Poling the piezoelectric material causes all the dipoles to align along the axis parallel to the direction of the applied electric field. This axis is termed as the polar axis and is generally referred to as the 3-direction. The energy harvesting performance depends on the direction of the applied strain relative to this polar axis. By symmetry, all directions in the plane at right angles to the polar axis are equivalent and are referred to as the 1-direction. A stress can be applied either in the direction of the polar axis or at right angles to it, resulting in two configurations commonly used for piezoelectric generators, termed 33-mode and 31-mode.

The most common design of an inertial piezoelectric energy harvester is a cantilever beam oscillating under the influence of harmonic base acceleration as shown in Fig. 1. Piezoelectric patches can be pasted along the length of the beam,

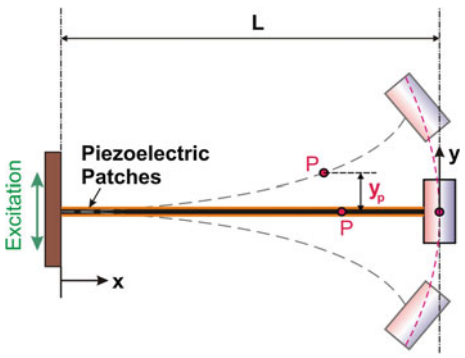

Fig. 1 Schematic representation of cantilever piezoelectric energy harvester

either in a unimorph or a bimorph configuration, to harvest electrical energy. The piezoelectric transducer, in this case, operates in 31-mode. The harvester can be modeled as a system of two coupled linear differential equations: one representing the mechanical domain and the other representing the electrical domain. The derivation of the governing differential equations is outlined here assuming a single degree-of-freedom (SDOF) approximation.

Consider a beam of length L, width b, thickness t, modulus of elasticity Y_b, and mass density ρ_b. Piezoelectric patches are pasted along the entire length of the beam as shown in Fig. 1. The width and thickness of the piezoelectric patches are b and t_p, respectively. Hence, the cross-sectional area of the composite harvester is given by $A = w(t + t_\mathrm{p})$. Let m_t be the mass of tip mass attached to the beam. Let $z = Z \sin \omega t$ be the base displacement. Let x denote the location of any point P along the length of the beam and $y_\mathrm{p}(x, t)$ denote the transverse displacement at the point P, at any time instant t. The transverse displacement of the tip mass is denoted by $y = y_\mathrm{p}(L, t)$. The beam deformation profile $\phi(x)$ relates the quantities y and y_p such that,

$$y_\mathrm{p}(x, t) = y(t) \cdot \phi(x) \tag{15}$$

Since we have assumed a single-mode approximation, we are only interested in the first mode of vibration of the beam. Hence, the beam deformation profile corresponds to the first mode of the solution of the eigenvalue problem,

$$Y_\mathrm{E} I \phi^{IV} + \rho A \phi = 0 \tag{16}$$

where Y_E, A, ρ, and I are the modulus of elasticity, area of cross section, density, and moment of inertia of the cross section of the composite beam.

The kinetic energy of the system is given as follows:

$$T = \frac{1}{2} m_t (\dot{y} + \dot{z})^2 + \frac{1}{2} \int_0^L \rho A (\dot{y}_p + \dot{z})^2 \mathrm{d}x \tag{17}$$

$$T = \frac{1}{2} \rho A \left[\dot{y}^2 \int_0^L (\phi(x))^2 \mathrm{d}x + \dot{z}^2 \int_0^L \mathrm{d}x + 2\dot{y}\dot{z} \int_0^L \phi(x) \mathrm{d}x \right] + \frac{1}{2} m_t \left[\dot{y}^2 + \dot{z}^2 + 2\dot{y}\dot{z} \right] \tag{18}$$

$$T = \frac{1}{2} (m\dot{y}^2 + M\dot{z}^2 + \mu \dot{y}\dot{z}) \tag{19}$$

where m, M, and μ are constants independent of time, such that

$$m = m_t + \rho A \int_0^L \phi^2 \mathrm{d}x \tag{20}$$

$$M = m_t + \rho A L \tag{21}$$

$$\mu = 2\left(m_t + \rho A \int_0^L \phi(x) \mathrm{d}x \right) \tag{22}$$

In the equations, overdot $(\cdot)$ denotes differentiation with respect to time.
The elastic potential energy of the system is given as follows:

$$\Pi_{\mathrm{E}} = \frac{1}{2} \int_0^L Y_{\mathrm{E}} I (\kappa(x,t))^2 \mathrm{d}x \tag{23}$$

where, $\kappa(x,t)$ is the curvature of the beam.
For the composite beam section, the moment of inertia is given as follows:

$$I = \frac{w(t+t_{\mathrm{p}})^3}{12} \tag{24}$$

The curvature of the beam is given as follows:

$$\kappa(x) = \frac{\mathrm{d}^2 y_{\mathrm{p}}}{\mathrm{d}x^2} \tag{25}$$

$$\kappa(x) = y \frac{\mathrm{d}^2 \phi}{\mathrm{d}x^2} \tag{26}$$

Substituting Eq. (26) into Eq. (23), we obtain the following:

$$\Pi_{\mathrm{E}} = \frac{1}{2} Y_{\mathrm{E}} I \left(y \int_0^L \frac{\mathrm{d}^2 \phi}{\mathrm{d}x^2} \mathrm{d}x \right)^2 \tag{27}$$

$$\Pi_{\mathrm{E}} = \frac{1}{2} Y_{\mathrm{E}} I y^2 (\phi'(L))^2 = \frac{1}{2} k y^2 \tag{28}$$

where $k = Y_{\mathrm{E}} I (\phi'(L))^2$ is the equivalent stiffness of the system.

The electrical work done in extracting the charges from the piezoelectric patches is given as follows:

$$W = \int_0^L M_\Lambda \kappa(x) \mathrm{d}x \tag{29}$$

where M_Λ is the moment due to the voltage developed across the piezoelectric patches and κ is the curvature of the beam.

Let v be the potential difference developed along the piezoelectric patches at any time instant t. For a bimorph configuration, the moment M_Λ produced due to this potential difference is given as follows:

$$M_\Lambda = Y_\mathrm{E} d_{31} w(t + t_\mathrm{p}) v \tag{30}$$

where d_{31} is the piezoelectric strain coefficient of piezoelectric patches.

On substituting Eqs. (26) and (30) into Eq. (29), we obtain the following:

$$W = Y_\mathrm{E} d_{31} w(t + t_\mathrm{p}) v \int_0^L y \frac{\mathrm{d}^2 \phi}{\mathrm{d}x^2} \mathrm{d}x \tag{31}$$

$$W = Y_\mathrm{E} d_{31} w(t + t_\mathrm{p}) v y \phi'(L) = Y_\mathrm{E} d_{31} \lambda v y \tag{32}$$

where

$$\lambda = w(t + t_\mathrm{p}) \phi'(L) \tag{33}$$

The total potential energy of the system is given as follows:

$$\Pi = \Pi_\mathrm{E} - W = \frac{1}{2} k y^2 - Y_\mathrm{E} d_{31} \lambda v y \tag{34}$$

Since the kinetic and potential energies of the system are known, the equation of motion can be derived using Euler–Lagrange equation:

$$\frac{\mathrm{d}}{\mathrm{d}t} \left(\frac{\partial L}{\partial \dot{y}} \right) - \frac{\partial L}{\partial y} = 0 \tag{35}$$

where $L = T - \Pi$ denotes the Lagrangian, which is the difference between kinetic and potential energies of the system.

On substituting Eqs. (19) and (34) into Eq. (35), the mechanical governing equation of the system can be obtained as follows:

$$m\ddot{y} + ky - Y_\mathrm{E} d_{31} \lambda v = -\mu \ddot{z} \tag{36}$$

Damping terms, such as viscous or material damping, can be added to the system defined in Eq. (36). On adding a viscous damping term, $c = 2\zeta\sqrt{km}$, the mechanical governing equation becomes:

$$m\ddot{y} + c\dot{y} + ky - Y_{\mathrm{E}} d_{31} \lambda v = -\mu\ddot{z} \tag{37}$$

The term $Y_{\mathrm{E}} d_{31} \lambda \dot{y}$ denotes the electromechanical coupling.

The electrical governing equation can be obtained by considering the piezoelectric patches to be a capacitor C_p connected across the load resistance R_{l}. Thus,

$$C_p \dot{v} + \frac{v}{R_{\mathrm{l}}} + Y_{\mathrm{E}} d_{31} \lambda \dot{y} = 0 \tag{38}$$

The term $Y_{\mathrm{E}} d_{31} \lambda \dot{y}$ arises due to the electromechanical coupling.

Equations (37) and (38) together represent the dynamics of a piezoelectric energy harvester based on a cantilever beam.

Assuming $y = Y\mathrm{e}^{i\omega t}$ and $v = V\mathrm{e}^{i\omega t}$ and performing a frequency-domain analysis on Eqs. (37) and (38) yield the following:

$$|V| = \left| \frac{\mu Y_{\mathrm{E}} d_{31} R_{\mathrm{l}} \lambda \omega^3 Z}{\sqrt{\left(k - m\omega^2 - C_p R_{\mathrm{l}} c\omega^2\right)^2 + \left(c\omega + R_{\mathrm{l}} \lambda^2 Y_{\mathrm{E}}^2 d_{31}^2 \omega - C_p R_{\mathrm{l}} m\omega^3 + C_p R_{\mathrm{l}} k\omega\right)^2}} \right| \tag{39}$$

The power harvested by the harvester over one cycle of excitation is given as follows:

$$P_{\mathrm{rms}} = \frac{\omega}{2\pi} \int_0^{2\pi/\omega} \frac{v^2}{R_{\mathrm{l}}} \mathrm{d}t = \frac{V^2}{2R_{\mathrm{l}}} \tag{40}$$

$$P_{\mathrm{rms}} = \frac{\left(\mu Y_{\mathrm{E}} d_{31} \lambda \omega^3 Z\right)^2 R_{\mathrm{l}}}{2\left[\left(k - m\omega^2 - C_p R_{\mathrm{l}} c\omega^2\right)^2 + \left(c\omega + R_{\mathrm{l}} \lambda^2 Y_{\mathrm{E}}^2 d_{31}^2 \omega - C_p R_{\mathrm{l}} m\omega^3 + C_p R_{\mathrm{l}} k\omega\right)^2\right]} \tag{41}$$

Equation (41) shows that the harvested power depends not only upon the material properties such as E and d_{31} but also on other factors such as load resistance R_{l} and capacitance of piezoelectric transducer C_{p}. However, we are only interested in a comparison of different materials for energy harvesting. Hence, we define a figure of merit F that depends only on the material properties as follows:

$$F = Y d_{31} \tag{42}$$

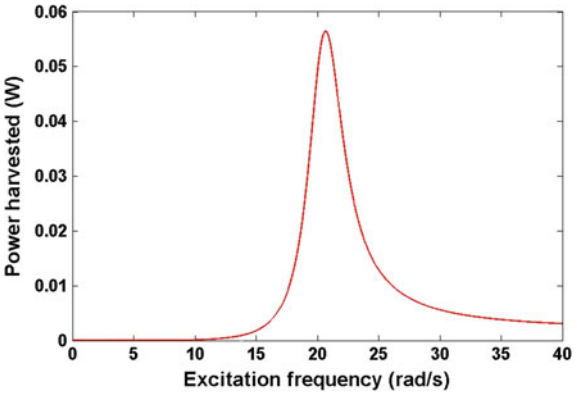

Fig. 2 Variation in harvested power with respect to frequency for a linear energy harvester employing a PVDF transducer

Thus, the power harvested can be related to the figure of merit as follows:

$$P_{\text{rms}} = \frac{(\mu F \lambda \omega^3 Z)^2 R_l}{2[(k - m\omega^2 - C_p R_l c\omega^2)^2 + (c\omega + R_l \lambda^2 F^2 \omega - C_p R_l m\omega^3 + C_p R_l k\omega)^2]} \tag{43}$$

The figure of merit defined in Eq. (42) is used to compare the harvesting properties of different electroactive polymers in Sect. 5.

Significant work has been done in the past in modeling cantilever-based linear piezoelectric energy harvesters (e.g., please refer [6, 13, 28, 29]). Such linear harvesters target a resonant design and suffer from poor efficiency at off-resonant frequencies as shown in Fig. 2.

To improve the operating bandwidth of kinetic vibration energy harvesters, techniques such as generator arrays, nonlinear oscillators, and active resonant tuning can be used [30]. Broadband piezoelectric energy harvesting techniques have been reviewed in [31]. Though the examples mentioned in [31] employ piezoelectric materials such as PZT, the design and analysis can be extended to harvesters employing PVDF or any other piezoelectric material by introducing appropriate changes in material properties.

3.2.2 Kinematic Energy Harvesters Using PVDF

While kinetic energy harvesters have a generic design in which there is a mass undergoing vibration, the design of kinematic energy harvesters is application specific. Kinematic energy harvesters are generally designed as an integral part of the host structure and deform along with the host structure. For example, a piezoelectric material can be coated on to the inner surface of a rubber tire. As the tire moves, the piezoelectric material deforms along with the tire and generates electrical energy. Generally, ductile piezoelectric materials such as PVDF are

employed in such applications. Modeling the dynamics of such harvesters, once again, would be application specific and hence not much research focus has been toward modeling such harvesters. But rather, modern research focuses on integrating kinematic energy harvesters as a part various commercial products such as tires, backpack straps [32], and footwear [33]. Significant efforts have also been made to harvest energy from biological processes such as respiration, walking, and squatting.

Another interesting area of application of kinematic energy harvesters is energy harvesting Eels. The design is based on bluff bodies and is intended to harvest energy from fluid–structure interaction [34, 35]. It converts the mechanical flow energy from oceans and rivers into electrical energy.

A comparison of various kinematic energy harvesters could be facilitated through a numerical model that takes into account the geometry, material properties, and other features of the harvester. However, since most of the kinematic energy harvesters are designed as an integral part of the structure and evaluated for their performance, not many studies related to modeling of such harvesters is available in the literature. Comparison of experimental data would not yield much information as the geometry and configuration of transducers used vary between different harvesters. Hence, a performance comparison between various transducer designs is not presented here per se, but a comparison of transducer materials based on their figure of merit is presented in Sect. 5.

3.2.3 Micro- and Nanogenerators Based on PVDF Composites

In addition to typical kinetic and kinematic energy harvesters, there is also significant opportunity to harvest the wasted energy from our daily activities, such as from walking, typing, speaking, and breathing. Energy harvested from such activities would range from few nanowatts to few microwatts, hence yielding such energy harvesters the name, micro- and nanogenerators.

Single-fiber PVDF nanowires [36], electrospun PVDF nanowebs, and nanowires made of semiconductive piezoelectric materials such as zinc oxide (ZnO) [37] are used as nanogenerators. ZnO nanowires have better electromechanical energy conversion efficiency than PVDF nanowires; but they are very brittle and are difficult to integrate with other most other materials. This has sparked the interest of researchers to develop a composite with PVDF matrix and ZnO nanoparticles to overcome the limitations associated with both the materials [38].

In such hybrid composites, PVDF nanowires provide the desired flexibility and the additive nanoparticles enhance the electromechanical coupling. Carbon nanotubes (CNTs) and piezoelectric ceramics such as $BaTiO_3$ and ZnO are some of the commonly used nanoparticles to improve the energy harvesting capabilities of PVDF nanogenerators. Figure 3 shows a nanogenerator that makes use of ZnO nanoparticles embedded in a PVDF nanofiber mat that is reported in [38].

Such flexible piezoelectric polymer–nanoparticle composites are generally manufactured using electro spinning process. The ingredients are dissolved in a

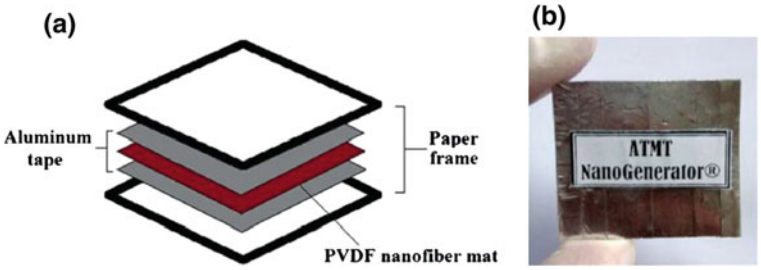

Fig. 3 Nanogenerator developed: **a** schematic diagram and **b** photograph of the actual device [38]. Copyright 2015. Reproduced with permission from Springer

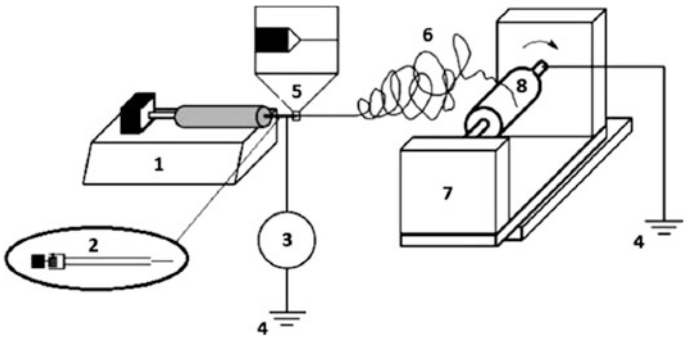

Fig. 4 Schematic diagram of the electrospinning process used for fabrication of PVDF nanofiber samples [38]. The numbers represent: (*1*) pump, (*2*) syringe, (*3*) high voltage supply, (*4*) ground, (*5*) Taylor cone, (*6*) draft zone, (*7*) frame of collector, and (*8*) rotary collector. Copyright 2015. Reproduced with permission from Springer

solvent such as acetone, and the solution is taken in a syringe pump. A high voltage is applied between the needle of the syringe and the collector. This would cause a fluid jet to be ejected from the needle. As the jet is accelerated, the solvent gets evaporated and the nanofibers get collected on the substrate. A schematic diagram describing the process is given by Fig. 4.

Apart from PVDF, polydimethylsiloxane (PDMS) and polyurethane (PU) are also used as matrix materials in such hybrid nanogenerators.

3.3 Energy Harvesting Using Cellulose Nanocrystals

Biopolymer electroactive materials such as cellulose nanocrystals are also explored for their energy harvesting capabilities owing to their low density, high mechanical strength, and most importantly their biocompatibility. The chemical resistance of cellulose ensures that it is not damaged by body fluids and its thermal stability

prevents fluctuating temperatures from altering its response. Hence, biocompatible composites made from cellulose nanocrystals have immense potential in the area of implantable energy harvesters. Such implantable energy harvesters would help to power cardiac pacemakers, enable targeted drug delivery through nanorobots, and aid in monitoring internal organs through biocompatible sensors.

Native cellulose, namely cellulose I, is the crystalline cellulose. The term, regenerated cellulose, is called cellulose II and usually needs a chemical treatment to prepare. The piezoelectric coupling constants depend on the crystallinity of the prepared cellulose. In general, the magnitude of the coupling constants increases with increase in crystallinity.

The network structure of cellulose consists of multiple OH groups in the glucose molecules from one chain forming hydrogen bonds with oxygen atoms in the same or neighboring chains. The hydrogen bonds hold the chains together side by side and are responsible for the spontaneous electric dipole formations in cellulose microfibrils inside the crystal lattice. The piezoelectric effect is produced by the displacement or reorientation of the dipoles in the crystal lattice under external stress [39].

In uniaxially oriented system of cellulose crystallites, relative movement between adjacent chains causes a reorientation of electric dipoles present in the crystal. The shear components predominantly contribute to relative movement between adjacent layers or chains. Hence, only the shear piezoelectric constants $-d_{14} = d_{25}$ are finite, while the other components are zero in a uniaxially oriented system of cellulose crystallites [40]. Hence, unlike the PVDF energy harvesters discussed so far which utilized either the 31- or 33-mode of coupling, energy harvesters based on cellulose nanocrystals make use of the shear mode of coupling.

In studies related to the piezoelectric behavior of cellulose fibers, different preparation and modification routes as well as characterization techniques have been considered. Corona-poled electroactive paper made from cellulose, cyanoethylated cellulose, and LiCl-DMAc-modified cotton (0.32 index of crystallinity) were reported to have shear piezoelectric constants of 0.0167, 0.01–0.02, and 0.016 nm/V, respectively.

Different designs of cellulose-based nanogenerators have been proposed in the past decade. The most prominent among such designs are described here. A nanogenerator based on cellulose-based electroactive paper was reported by [41]. In this design, the electromechanical coupling was enhanced through fiber functionalization that involves anchoring nanostructured $BaTiO_3$ into a stable matrix with wood cellulose fibers. The electroactive paper has the largest piezoelectric coefficient, $d_{33} = 4.8 \pm 0.4\ pC/N$, at the highest nanoparticle loading of 48% $BaTiO_3$ by weight [41].

A flexible nanogenerator based on native cellulose microfiber and polydimethylsiloxane embedded with multi-wall carbon nanotubes as filler was proposed by [42]. It delivers a high electrical throughput that is an open-circuit voltage of 30 V and power density of 9.0 $\mu W/cm^3$ under repeated hand punching. This design utilized naturally available cellulose fibers and avoided chemical post-processing treatment and electrical poling.

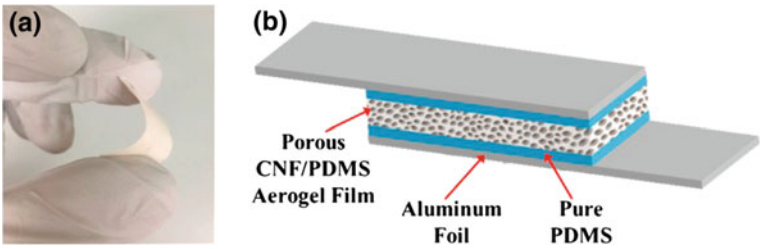

Fig. 5 **a** Photograph of the flexible porous CNF-PDMS aerogel film. **b** A schematic diagram of the CNF-PDMS aerogel film-based nanogenerator [43]. Copyright 2016. Reproduced with permission from Elsevier

Another flexible nanogenerator based on porous cellulose nanofibrils–polydimethylsiloxane (CNF–PDMS) aerogels was proposed by [43]. The design consists of three layers, namely the inner-most CNF-PDMS layer sandwiched between two thin PDMS films followed by two aluminum foils as shown in Fig. 5. The inner CNF-PDMS layer was produced by coating a layer of PDMS onto a compressed CNF aerogel film through a freeze–drying process. This nanogenerator exhibited very stable and high electrical output with an open-circuit voltage of 60.2 V, a short-circuit current of 10.1 μA, and a corresponding power density of 6.3 mW/cm^3.

Apart from the ones mentioned above, feasibility and performance studies on energy harvesting using ultra-thin cellulose nanocrystal films, hybrid cellulose–polydimethylsiloxane composites, etc., are underway.

4 Energy Harvesting from Electrostrictive Polymers

Electrostrictive materials are those in which the electromechanical coupling is represented by a quadratic relationship between strain and electric field [23]. In tensorial notation, the relation between strain and electric field is written as follows[44]:

$$\varepsilon_{ij} = S_{ijkl}\sigma_{kl} + M_{ijmn}E_mE_n \tag{44}$$

$$D_m = \kappa_{mn}E_n + 2M_{mnij}E_n\sigma_{ij} \tag{45}$$

where M_{ijmn} is a fourth rank tensor of electrostriction coefficients.

On considering only the 31 lateral vibration mode coupling, the constitutive equations reduce to [44]:

$$\varepsilon_1 = S_{11}\sigma_1 + M_{31}E_1^2 \tag{46}$$

$$D_3 = \kappa_{33}E_3 + 2M_{31}E_3\sigma_1 \tag{47}$$

where the input and response fields and associated material properties are expressed in Voigt notation.

In piezoelectric materials, linear coupling between strain and electric field produces a mechanical response that will change polarity when the polarity of the electric field is changed. On the other hand, electrostrictive materials, due to the quadratic dependence of strain on electric field relationship, always produce strain in only a single direction, irrespective of the polarity of the applied electric field.

Ceramics such as lead lanthanum zirconate titanate (PLZT), lead magnesium niobate (PMN) and a solid solution of lead magnesium niobate–lead titanate (PMN-PT) and polymers such as polyurethane (PU) and polymethyl dioxane are some common examples of electrostrictive materials.

4.1 Effect of Intrinsic Mechanisms

Analogous to electrostriction, there is another phenomenon observed widely in soft dielectric elastomers where the strain is proportional to the square of the electric field. This phenomenon is known as the Maxwell stress effect. The Maxwell stress is a result of the electrostatic forces between the free charges on the electrodes of a sample. Apart from Maxwell stress effect, other intrinsic mechanisms such as Joule's heating effect and space charge effect also contribute to the strain. To take into account all the intrinsic mechanisms that contribute to the strain, the true electrostrictive coefficient M_{31} must be replaced with the apparent electrostrictive coefficient M_{31}^*, which is defined as follows [45]:

$$M_{31}^* = M_{31} + M_{31}^M + M_{31}^T \tag{48}$$

where M_{31}^M and M_{31}^T denote the contributions from Maxwell stress effect and Joule's heating effect, respectively.

Now, the constitutive Eqs. (46) and (47) can be redefined as follows:

$$\varepsilon_1 = S_{11}\sigma_1 + M_{31}^*E_1^2 \tag{49}$$

$$D_3 = \kappa_{33}E_3 + 2M_{31}^*E_3\sigma_1. \tag{50}$$

4.2 Tackling Quadratic Dependence of Strain on Electric Field

The quadratic relationship between applied electric field and mechanical strain complicates the design of transducers based on electrostrictive materials. In an electrostrictive material, the spontaneous polarization is always zero. When the electrostrictive material is strained, some of the dipoles orient along a particular direction and the rest orient along the opposite direction, thus reducing the net polarization, as shown in Fig. 6.

One method of avoiding this is to apply a high dc bias voltage to the material along the desired direction of electrical response. The dc electric field will force the dipoles to orient in a direction parallel to it. Hence, to get a full cycle alternating current as output, electrostrictive energy harvesters require a dc bias field to be applied, while piezoelectric harvesters do not. This forms the essential difference between the operating principles of electrostrictive energy harvesters and their piezoelectric counterparts.

Continuing with our analysis, consider the electric field in the 3-direction to be the sum of a direct current (dc) bias field and an induced alternating current (ac) component:

$$E_3 = E_{\mathrm{dc}} + E_{\mathrm{ac}} \tag{51}$$

Substituting Eq. (51) into Eq. (49) yields

$$\varepsilon_1 = S_{11}\sigma_1 + M_{31}^{*}(E_{\mathrm{dc}} + E_{\mathrm{ac}})^2 \tag{52}$$

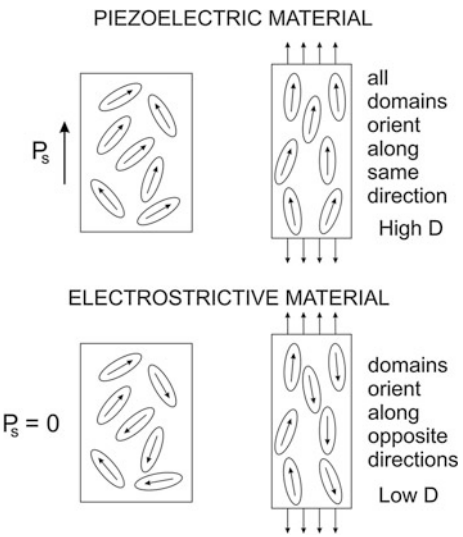

Fig. 6 Alignment of dipoles in response to applied strain in piezoelectric and electrostrictive materials

$$\varepsilon_1 = S_{11}\sigma_1 + M_{31}^*(E_{dc}^2 + 2E_{dc}E_{ac} + E_{ac}^2) \tag{53}$$

$$\varepsilon_1 - M_{31}^* E_{dc}^2 = S_{11}\sigma_1 + M_{31}^*(2E_{dc}E_{ac} + E_{ac}^2) \tag{54}$$

When $E_{ac}^2 \ll E_{dc}E_{ac}$, Eq. (54) can be approximated as follows:

$$\varepsilon_1 - M_{31}^* E_{dc}^2 \approx S_{11}\sigma_1 + 2M_{31}^* E_{dc}E_{ac} \tag{55}$$

The noteworthy fact in Eq. (55) is that the ac strain $(\varepsilon_1 - M_{31}^* E_{dc}^2)$ is a linear function of the ac field E_{ac} when a sufficiently large dc bias field E_{dc} is applied to the system. While the strain ε_1 can only be positive, the ac strain can be either positive or negative depending on the value of $M_{31}^* E_{dc}^2$. Thus, the relationship between ac strain and ac electric field in electrostrictive materials is similar to that of strain and electric field in piezoelectric materials.

Moreover, in Eq. (55), the coefficient $2M_{31}^* E_{dc}$ is constant as the applied dc field is constant with time. This leads to the notion of comparing Eq. (55) with that of the linear piezoelectric constitutive relations to express $d^* = 2M_{31}^* E_{dc}$ as the effective piezoelectric strain coefficient. This would be helpful in comparing the electromechanical transduction capability of electrostrictive materials with that of piezoelectric materials.

4.3 Energy Harvesting Using Polyurethane Transducers

Similar to piezoelectric transducers, electrostrictive transducers are widely used in kinetic energy harvesting. However, the requirement of a dc bias field limits the use of electrostrictive polymers in kinematic energy harvesting, as it is highly challenging to apply a uniform bias field over irregular membranes of electrostrictive materials pasted onto the surface of the host.

The modeling and analysis of kinetic electrostrictive energy harvesters also differ from their piezoelectric counterparts. Modeling of a cantilever-based electrostrictive energy harvester, similar to the one discussed for piezoelectric energy harvesting, is elucidated here.

Consider a cantilever beam of length L, cross-sectional area A, and modulus of elasticity E. Electrostrictive transducers are pasted in a bimorph configuration onto the beam as shown in Fig. 7. The transducer operates in 31-mode. A dc bias field of magnitude E_{dc} is applied to the transducer along the positive 3-direction. Due to the base excitation, the beam undergoes transverse vibrations along 1-direction.

The transducer equations are given as follows:

$$\varepsilon_1 = S_{11}\sigma_1 + M_{31}^*(E_{dc} + E_{ac})^2 \tag{56}$$

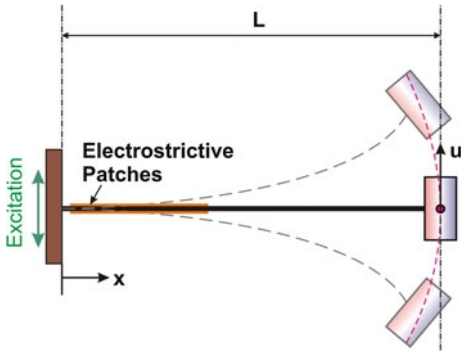

Fig. 7 Schematic representation of cantilever electrostrictive energy harvester

$$D_3 = \kappa_{33}(E_{dc} + E_{ac}) + 2M_{31}^{*}(E_{dc} + E_{ac})\sigma_1 \tag{57}$$

The harvested current I is the rate of change of total charge displaced. Hence,

$$I = \dot{q} \tag{58}$$

$$I = A_e D \tag{59}$$

$$I = A_e(\kappa_{33}E_{ac} + 2M_{31}^{*}E_{ac}\sigma_1 + 2M_{31}^{*}(E_{ac} + E_{dc})\dot{\sigma}_1) \tag{60}$$

$$I = A_e\left[[\kappa_{33} + 2M_{31}^{*}\sigma_1]E_{ac} + 2M_{31}^{*}(E_{ac} + E_{dc})\dot{\sigma}_1\right] \tag{61}$$

$$I = A_e\left[\left[\kappa_{33} - 6\frac{M_{31}^{*2}}{S_{11}}(E_{ac} + E_{dc})^2 + \frac{2M_{31}^{*2}}{S_{11}}\varepsilon_1\right]\dot{E}_{ac} + \frac{2M_{31}^{*2}}{S_{11}}(E_{ac} + E_{dc})\dot{\varepsilon}_1\right] \tag{62}$$

where A_e is the area of the electrode of the electrostrictive transducer.

For practically realizable values of current ($I < 100\,\mu A$), load resistance ($R_l < 10^7\,\Omega$), and electric field (1–100 MV/m), the ac component E_{ac} can be neglected when compared to the dc bias field. Hence, Eq. (62) becomes:

$$I = A_e\left[\left[\kappa_{33} - 6\frac{M_{31}^{*2}}{S_{11}}E_{dc}^2 + \frac{2M_{31}^{*2}}{S_{11}}\varepsilon_1\right]\dot{E}_{ac} + \frac{2M_{31}^{*2}}{S_{11}}E_{dc}\dot{\varepsilon}_1\right] \tag{63}$$

If t_p is the thickness of the electrostrictive transducer, then the potential difference across the transducer and the corresponding electric field are related by:

$$E_{ac} = \frac{v}{t_p} = \frac{IR_l}{t_p} \tag{64}$$

where R_l is the load resistance.

Substituting Eq. (64) into Eq. (63) yields

$$I = \frac{A_e R_l}{t_p}\left[\kappa_{33} - 6\frac{M_{31}^{*2}}{S_{11}}E_{dc}^2 + 2\frac{M_{31}^*}{S_{11}}\varepsilon_1\right]I + \frac{2M_{31}^* A_e}{S_{11}}E_{dc}\dot{\varepsilon}_1 \tag{65}$$

For small values of strain (a few percent), the terms $6\frac{M_{31}^{*2}}{S_{11}}E_{dc}^2$ and $2\frac{M_{31}^*}{S_{11}}\varepsilon_1$ are very small in magnitude compared to permittivity κ_{33} and can be neglected [46]. Thus,

$$I = \frac{A_e R_l}{t_p}\kappa_{33} I + \frac{2M_{31}^* A_e}{S_{11}}E_{dc}\dot{\varepsilon}_1 \tag{66}$$

On setting $\varepsilon_1 = \varepsilon_m e^{i\omega t}$ and $I = I_m e^{i\omega t}$, the frequency-domain analysis of Eq. (66) yields [46]:

$$|I_m| = \left|\frac{A_e M_{31}^* E_{dc} t_p}{S_{11}\sqrt{t_p^2 + (\omega\kappa_{33}R_l A_e)^2}}\varepsilon_m^2\right| \tag{67}$$

The power harvested over one cycle is then given as follows:

$$P_{rms} = \frac{1}{2}I_m^2 R_l \tag{68}$$

$$P_{rms} = \frac{(A_e M_{31}^* E_{dc} t_p)^2}{2S_{11}^2(t_p^2 + (\omega\kappa_{33}A_e R_l)^2)}\varepsilon_m^2 \tag{69}$$

Since the effective piezoelectric strain coefficient is defined as $d^* = 2M_{31}^* E_{dc}$, a figure of merit, equivalent to the one defined for piezoelectric materials, can also be defined for electrostrictive materials. In Eq. (42), replacing d_{31}^* with d_{31}, we obtained the following:

$$F = d_{31}^* Y \tag{70}$$

$$F = \frac{2M_{31}^* E_{dc}}{S_{11}} \tag{71}$$

From Eq. (71), we observe that the figure of merit for an electrostrictive material also depends on the dc bias field. This is expected because higher the dc bias field, higher will be the net polarization in the electrostrictive material. However, the net polarization will not increase beyond a certain limiting value of the dc bias field known as the saturation field E_s. Hence, the maximum permissible value of figure of merit is obtained when $E_{dc} = E_s$.

The power harvested and the figure of merit are related by:

$$P_{\text{rms}} = \frac{(FA_e t_p)^2 R_l}{8(t_p^2 + (\omega \kappa_{33} R_l A_e)^2)} \varepsilon_m^2 \tag{72}$$

The figure of merit defined in Eq. (71) is used to compare the harvesting properties of different electroactive polymers in Sect. 5.

The variation in harvested power with respect to load resistance R_l and strain amplitude ε_m for three different polyurethane composites is shown in Figs. 8 and 9, respectively. Pure polyurethane (PU), polyurethane embedded with 0.5% SiC nanowires (PU with 0.5% SiC), and polyurethane embedded with 1% carbon nanopowder (PU with 1% C) are the three materials chosen for study. The material properties used are given in Table 2. The excitation frequency, dc bias field,

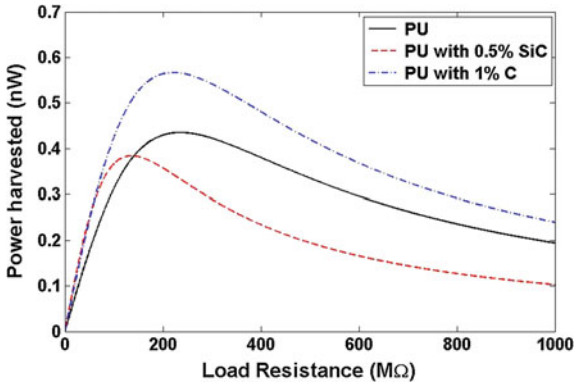

Fig. 8 Variation in harvested power with respect to load resistance for various polyurethane composites. The strain amplitude is taken to be 1%

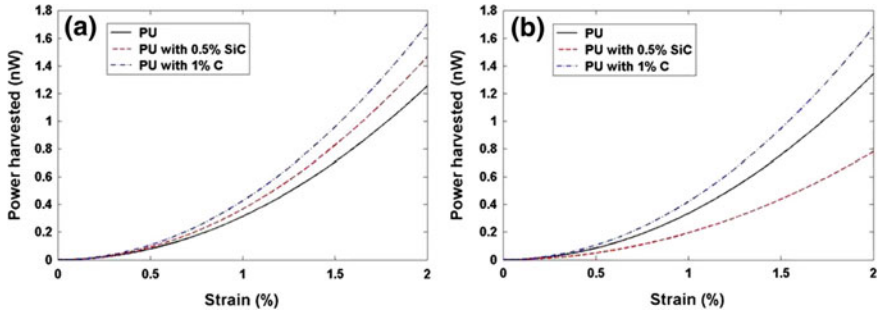

Fig. 9 Variation in harvested power with respect to strain for various polyurethane composites for a load resistance of **a** 100 MW and **b** 500 MW

Table 2 Comparison of electromechanical properties of various dielectric EAPs

Material	Modulus of elasticity (MPa)	Relative dielectric permittivity	Apparent electrostrictive coefficient (10^{-18} m^2/V^2)	Effective piezoelectric strain coefficient (10^{-12} pC/N)	Figure of merit (mC/m^2)
PU [47]	40	4.8	3.4	27.2	1.088
PU 0.5% SiC [47]	80	5.1	2.0	16	1.28
PU 1% C [47]	40	8.3	4.2	33.6	1.344
Polyethylene [47]	260	2.2	0.34	2.72	0.7072
Nylon [47]	2800	12	0.14	1.12	3.136
PVDF [48]	2600	12	–	37	96.2
PZT [23]	74000	1800	–	−175	−12950

The references are indicated in the first column

electrode surface area, and thickness of transducer are taken to be 10 rad/s, 4 MV/m, 5 cm^2, and 50 μm, respectively, for all the three cases.

As shown in Fig. 8, the power harvested is maximum corresponding to certain optimal load resistance. This optimal resistance is a function of material properties and is given by the expression $R_{opt} = (A_e \kappa_{33} \omega)^{-1}$ [46]. For more details on the optimization procedure and the corresponding maximum value of power harvested, please refer [46].

From Fig. 8, it is observed that the composite PU with 0.5% SiC performs better than PU in terms of power harvested for all load resistance levels. On the other hand, the composite PU with 1% C harvests more power than PU for lower resistances (<120 MΩ approx.) and harvests less power than PU for higher resistances. The same is reflected in Fig. 9. Figure 9 also shows that the harvested power varies quadratically with strain for all the three materials.

5 Comparison of Electromechanical Coupling in Various Dielectric EAPs

The apparent electrostrictive coefficient M_{31}^* is a measure of the mechanical-to-electrical energy conversion in electrostrictive materials. To increase the apparent electrostrictive coefficient of polyurethane, particles such as carbon black nanopowders or silicon carbide nanowires can be added to a polyurethane matrix [45, 47]. Co-polymerization of certain combination of monomers can also significantly improve the electromechanical coupling. For example, the co-polymer P (VDF-TrFE) has better electromechanical coupling properties than PVDF. However, a direct comparison cannot be made between the piezoelectric strain

coefficient of ferroelectric polymers and the apparent electrostrictive coefficient of electrostrictive polymers.

To facilitate the comparison between various dielectric EAPs, the notion of effective piezoelectric strain coefficient introduced in Sect. 4.2 can be used. Table 2 compares the effective piezoelectric strain coefficient of various electrostrictive polymers with that of the piezoelectric materials. To compare the energy harvesting efficiency of the materials, figure of merit defined in Eqs. (42) and (71) is used. To calculate the effective piezoelectric strain coefficient d_{31}^{*} and figure of merit F for electrostrictive materials, a dc bias field value of 4 MV/m is used.

Even though dielectric EAPs feature a very low figure of merit when compared to PZT, they are still used in energy harvesting applications due to their flexibility, maneuverability, and affordability.

6 Energy Harvesting from Conductive Polymer Composites

Conducting polymers are materials that exhibit a reversible volume change due to electrochemical reactions caused by the introduction and removal of ions into the polymer matrix [23]. A conductive polymer transducer consists of the conducting polymer material, an electrolyte that serves as a source of ions, and two electrodes that control the ionic diffusion. Polypyrrole, poly(p-phenylene), and several other polymers based on aromatic monomers such as thiopene and aniline when doped act as the conducting polymer material.

Application of a potential difference between the two electrodes causes an electrochemical redox reaction, which in turn causes a volume change inside the conducting polymer. The volume change in the conducting polymer results in its mechanical deformation. The deformation of the polymer film is used to provide the actuation strain. This phenomenon is called the electro-chemo-mechanical (ECM) deformation as it involves transformation of electrical energy to kinetic energy through a chemical reaction. The reversal process in which kinetic energy is transformed into electrical energy is observed experimentally toward the end of twentieth century by Takashima et al. [25]. The reversal effect, called the mechano-chemo-electrical (MCE) effect, can be utilized for sensing and energy harvesting applications. The kinetic-to-electrical energy conversion efficiency, as reported in [25], is less than 0.01%.

Owing to the very low MCE conversion efficiency of conducting polymers such as polyaniline and polypyrrole, they are not as such used in mechanical energy harvesting. Instead, they are used as electrodes in microbial fuel cells [49] and thermoelectric energy harvesters [50], and also as fillers in hybrid polymer-nanoparticle energy harvesters [51].

Apart from conducting polymers, composites consisting of conductive nanoparticles such as carbon nanotubes (CNTs) dispersed in a polymer matrix also fall under the category of conducting polymer composites.

Mechanical energy harvesting from such hybrid polymer–nanoparticle composites has been elucidated in Sect. 3.2.3. Apart from that, thermoelectric energy harvesters with carbon nanotube electrodes are one of the modern state-of-the-art technological devices where active research is going on. A brief review of latest advancements in their design and the perspectives is elucidated next.

6.1 Thermoelectric Energy Harvesters with Carbon Nanotube Electrodes

Carbon nanotubes (CNTs) were first discovered in 1953 through research in the Soviet Union, but the first accessible results were by Sumio Iijima in 1991 as a result of research into Buckminster fullerenes. CNTs have a cylindrical shape that can be considered as a grapheme sheet rolled up, either individually as a single-walled carbon nanotube (SWNT), or concentrically as a multi-walled carbon nanotube (MWNT) [52]. They exhibit remarkable electrical transport and mechanical properties, which is why interest and research into this material has increased over the last two decades.

The second law of thermodynamics dictates that a heat engine can never have perfect efficiency and will always produce surplus heat. This waste heat (or low-grade heat) is one of the world's most ubiquitous sources of untapped energy. For instance, nearly 70% of the energy produced by burning fuel in an IC engine ends up as waste heat energy in the form of hot exhaust gases and heated up engine components.

To convert such low-grade heat into electrical energy, a thermogalvanic cell, also known as a thermocell is used. A thermocell is an energy converter that utilizes electrochemical reactions to attain conversion of low-grade heat to electrical power. It operates based on the Seebeck effect. The two half cells of the system are held at different temperatures causing a difference in redox potentials of the mediator at the anode and cathode. This reaction can drive electrons through an external circuit that allows generation of current and power.

The thermal power flowing through the cell is largely controlled by cell design and electrolyte selection. When a reversible redox couple is used, no net consumption of the electrolyte occurs. Hence, typically, ferri/ferrocyanide redox couple is used as the electrolyte. The Seebeck coefficient of ferri/ferrocyanide redox couple is 1.4 mV/K. This implies that an open-circuit potential of 1.4 mV is attainable at a thermal gradient of 1 K. A schematic of a thermocell with a ferri/ferrocyanide redox couple is shown in Fig. 10. The redox reactions occurring at the electrodes are also indicated therein.

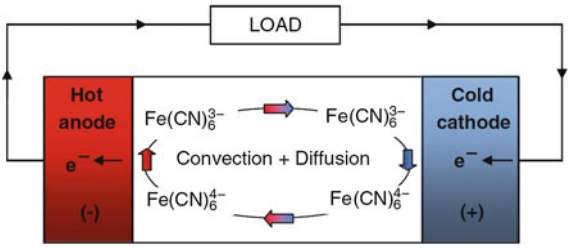

Fig. 10 Ferri/ferrocyanide redox couple thermogalvanic cell [53]. Copyright 2012. Reproduced with permission from Springer

Ferrocyanide is oxidized at the hot anode; the electron generated then travels through an external circuit and returns to the cell via the cold cathode where it is consumed in the reduction of ferricyanide. The accumulation of reaction products at half cell is prevented either by the diffusion or by the convection of the electrolyte that occurs naturally, thus eliminating the need for moving mechanical components.

The cell design should be such that it reduces the voltages losses occurring in the cell. Typically, voltage losses occur in the form of ohmic, mass transport, and activation overpotentials. Ohmic overpotential is the voltage loss due to resistance offered by the electrolyte, and mass transport overpotential is the loss incurred due to the time taken for the movement of ions within the electrolyte. Minimizing the distance between the electrodes would decrease the resistance and hence reduce the ohmic overpotential. Minimizing the distance would also reduce the time taken for ions to travel from one electrode to the other, thus reducing the mass transport overpotential. However, the distance between electrodes cannot be reduced beyond a certain limit as it would be hard to maintain the temperature gradient between the anode and the cathode. Hence, the electrode distance has to be fixed so as to achieve a balance between the two.

Activation overpotential is associated with the activation barrier needed to be overcome to start a reaction. For the same activation overpotential, larger current densities are realized when the exchange current density is increased. This increase is attained when the concentration of the redox couple in the electrolyte is maximized, the thermal gradient is increased, and the number of possible reaction sites is augmented. Porous electrodes have the advantage of increased electroactive surface area and will directly amplify the short-circuit current density.

This is where carbon nanotubes could play a significant role in improving the efficiency of thermogalvanic cells. The diameter of CNTs is of the range of few nanometers, and this gives rise to large gravimetric and volumetric specific surface areas (SSA). Their unique aspect ratios allow porous electrodes to be fabricated by a variety of methods. Also, CNT electrodes exhibit fast electron transfer kinetics with the redox couple ferri/ferrocyanide. This justifies the use of CNTs as electrodes in ferri/ferrocyanide thermo cells.

It has been demonstrated that the efficiency of thermocells with MWNT electrodes is high as 1.4% relative to the Carnot Cycle, which is three times higher than the efficiency of conventional thermocell devices with platinum electrodes [54]. This efficiency was raised to 2.6% by introducing a carbon SWNT/reduced

graphene oxide (rGO) composite electrode [55]. Improved mass transport due to enhanced porosity of the optimized SWNT/rGO composite was found responsible for the efficiency enhancement.

To improve this efficiency further to 3.95%, the following strategies have been deployed: the use of CNT aerogel sheets as electrodes, removal of low activity carbonaceous impurities that limit electron transfer kinetics, decoration of CNT sheets with catalytic platinum nanoparticles, mechanical compression of nanotube sheets to tune conductivity and porosity, and the utilization of a cylindrical cell geometry [56]. The use of aerogel sheets would increase the porosity, and the addition of catalytic particles and removal of low activity impurities would lower the activation overpotential, thereby leading to an increase in the overall efficiency.

Apart from CNT nanotube and aerogel electrodes, polymer electrodes embedded with CNTs have also been explored for the use in thermocells. A detailed review of such composite electrodes is presented in [57].

The prime challenge faced by the research community in thermoelectric energy harvesting is that the Carnot-relative efficiency should be around 5% for commercial viability of such harvesters. Hence, new methods of improving the efficiency of thermocells are under exploration.

7 Summary

Electroactive polymers offer the possibility of developing new high-performance, flexible energy harvesters. EAPs can be broadly classified into two categories: dielectric EAPs and ionic EAPs. Conductive polymer composites fall under the category of ionic EAPs, whereas most of the crystalline and semicrystalline polymers fall under the category of dielectric EAPs. The dielectric EAPs can be further classified into ferroelectric and electrostrictive based on their stain–electric field relationship.

As far as conductive polymer composites are concerned, their efficiency in terms of mechanical-to-electrical energy is very low. This is because, the energy conversion from mechanical to electrical is not direct but mediated through a chemical reaction. Hence, their use as transducers in mechanical energy harvesters is not efficient. However, conductive polymers with carbon nanotube fillers are excellent candidates for making electrodes of thermogalvanic cells owing to their low manufacturing cost, chemical and thermal stability, and fast electron transfer kinetics.

The Carnot-relative efficiency achieved so far in CNT-based thermocells is 3.95%. However, for commercial viability, the efficiently still needs to be improved, so as to achieve 5% Carnot-relative efficiency.

Crystalline and semicrystalline dielectric EAPs are widely used as transducers in mechanical energy harvesting. In the context of kinematic energy harvesting, wherein the harvesters could be designed as an integral part of the host structure, the use of ferroelectric PVDF transducers is highly promising. This can be

attributed to the fact that PVDF is very flexible and also possesses high piezoelectric strain coefficient than other polymers.

The use of electrostrictive polymers such as polyurethane and composites of polyurethane is highly encouraged in kinetic energy harvesting as they have high electromechanical coupling. However, the need for a dc bias field for operation is a limitation to electrostrictive transducers. In cases where application of a dc bias field is difficult, piezoelectric polymers such as PVDF could be employed.

Biopolymers such as cellulose nanocrystals are explored for their energy harvesting capabilities primarily because of their biocompatibility. They could be used to design implantable energy harvesters that could power pacemakers, targeted drug delivery systems, etc. Low density, high strength ease of availability, chemical resistance, and thermal stability of cellulose nanocrystals also contribute to their viability in mechanical energy harvesting.

The challenges facing the field of implantable energy harvesters are the legal issues concerned with performing in vitro experiments on living organisms. Though many prototypes have been designed and tested using laboratory equipment, the performance of such harvesters while being implanted into the host organism is yet to be explored.

To sum up, dielectric EAPs, both ferroelectric and electrostrictive, offer good performance levels in mechanical energy harvesting, whereas conductive polymer composites find more applications in the field of thermoelectric energy harvesting.

References

1. Kim H, Tadesse Y, Priya S (2009) Piezoelectric energy harvesting. Energy harvesting technologies. Springer, US, pp 3–39
2. Qi Y, Jafferis NT, Lyons K et al (2010) Piezoelectric ribbons printed onto rubber for flexible energy conversion. Nano Lett 10:524–528
3. Inman DJ, Erturk A, Inman DJ (2011) Piezoelectric energy harvesting. Wiley, USA
4. Mane P, Jingsi Xie J, Leang KK, Mossi K (2011) Cyclic energy harvesting from pyroelectric materials. IEEE Trans Ultrason Ferroelectr Freq Control 58:10–17
5. Bowen CR, Kim HA, Weaver PM, Dunn S (2014) Piezoelectric and ferroelectric materials and structures for energy harvesting applications. Energy Environ Sci 7:25
6. Erturk A, Inman DJ (2009) An experimentally validated bimorph cantilever model for piezoelectric energy harvesting from base excitations. Smart Mater Struct 18:025009
7. Friswell MI, Ali SF, Bilgen O et al (2012) Non-linear piezoelectric vibration energy harvesting from a vertical cantilever beam with tip mass. J Intell Mater Syst Struct 23:1505–1521
8. Ma TW, Zhang H, Xu NS (2012) A novel parametrically excited non-linear energy harvester. Mech Syst Signal Process 28:323–332
9. Malaji PV, Ali SF (2015) Analysis of energy harvesting from multiple pendulums with and without mechanical coupling. Eur Phys J Spec Top 224:2823–2838
10. Zhou S, Cao J, Inman DJ et al (2014) Broadband tristable energy harvester: modeling and experiment verification. Appl Energy 133:33–39

11. Aravind Kumar K, Ali SF, Arockiarajan A (2015) Piezomagnetoelastic broadband energy harvester: nonlinear modeling and characterization. Eur Phys J Spec Top. doi:10.1140/epjst/e2015-02590-8
12. Erturk A, Hoffmann J, Inman DJ (2009) A piezomagnetoelastic structure for broadband vibration energy harvesting. Appl Phys Lett 94:254102
13. Williams CB, Yates RB (1995) Analysis of a micro-electric generator for microsystems. Proc Int Solid-State Sens Actuators Conf TRANSDUCERS '95 1:8–11
14. Kim SG, Priya S, Kanno I (2012) Piezoelectric MEMS for energy harvesting. MRS Bull 37:1039–1050
15. Leo DJ (2007) Engineering analysis of smart material systems. Wiley, USA
16. Bar-Cohen Y (2004) Electroactive polymer (EAP) actuators as artificial muscles: reality, potential, and challenges. SPIE Press, USA
17. Kornbluh RD, Flamm DS, Prahlad H, et al (2003) Shape control of large lightweight mirrors with dielectric elastomer actuation. In: Bar-Cohen Y (ed) International society for optics and photonics, p 143
18. Krishen K (2009) Space applications for ionic polymer-metal composite sensors, actuators, and artificial muscles. Acta Astronaut 64:1160–1166
19. Menon C, Carpi F, De Rossi D (2009) Concept design of novel bio-inspired distributed actuators for space applications. Acta Astronaut 65:825–833
20. Shahinpoor M, Kim KJ, R BP, et al (2005) Ionic polymer–metal composites: IV. Industrial and medical applications. Smart Mater Struct 14:197–214
21. Wax SG, Sands RR (1999) Electroactive polymer actuators and devices. In: Bar-Cohen Y (ed) International society for optics and photonics, pp 2–10
22. Kovacs G, Lochmatter P, Wissler M et al (2007) An arm wrestling robot driven by dielectric elastomer actuators. Smart Mater Struct 16:S306–S317
23. Smith RC (2005) Smart material systems. Society for Industrial and Applied Mathematics
24. Jean-Mistral C, Basrour S, Chaillout J-J (2010) Comparison of electroactive polymers for energy scavenging applications. Smart Mater Struct 19:085012
25. Takashima W, Uesugi T, Fukui M et al (1997) Mechanochemoelectrical effect of polyaniline film. Synth Met 85:1395–1396
26. Vinogradov A (2002) Piezoelectricity in Polymers. In: Encyclopedia of smart materials. Wiley, USA
27. Sessler GM (1982) Chapter 6—polymeric electrets. In: electrical properties of polymers, pp 241–284
28. Erturk A, Inman DJ (2009) Electromechanical modeling of cantilevered piezoelectric energy harvesters for persistent base motions. Energ Harvesting Technol. Springer, US, pp 41–77
29. Roundy S, Wright PK, Rabaey J (2003) A study of low level vibrations as a power source for wireless sensor nodes. Comput Commun 26:1131–1144
30. Twiefel J, Westermann H (2013) Survey on broadband techniques for vibration energy harvesting. J Intell Mater Syst Struct 24:1291–1302
31. Tang L, Yang Y, Soh CK (2010) Toward broadband vibration-based energy harvesting. J Intell Mater Syst Struct 21:1867–1897
32. Granstrom J, Feenstra J, Sodano H, Farinholt K (2007) Energy harvesting from a backpack instrumented with piezoelectric shoulder straps. Smart Mater Struct 16:1810–1820
33. Rocha JG, Gonçalves LM, Rocha PF et al (2010) Energy harvesting from piezoelectric materials fully integrated in footwear. IEEE Trans Ind Electron 57:813–819
34. Taylor GW, Burns JR, Kammann SM et al (2001) The energy harvesting Eel: A small subsurface ocean/river power generator. IEEE J Ocean Eng 26:539–547
35. Allen JJ, Smits AJ (2001) Energ Harvesting Eel J Fluids Struct 15:629–640
36. Hansen BJ, Liu Y, Yang R, Wang ZL (2010) Hybrid nanogenerator for concurrently harvesting biomechanical and biochemical energy. ACS Nano 4:3647–3652
37. Yang R, Qin Y, Dai L, Wang ZL (2009) Power generation with laterally packaged piezoelectric fine wires. Nat Nanotechnol 4:34–39

38. Sorayani Bafqi MS, Bagherzadeh R, Latifi M (2015) Fabrication of composite PVDF-ZnO nanofiber mats by electrospinning for energy scavenging application with enhanced efficiency. J Polym Res 22:130
39. Fukada E (1968) Piezoelectricity as a fundamental property of wood. Wood Sci Technol 2:299–307
40. Csoka L, Hoeger IC, Rojas OJ et al (2012) Piezoelectric effect of cellulose nanocrystals thin films. ACS Macro Lett 1:867–870
41. Mahadeva SK, Walus K, Stoeber B (2014) Piezoelectric paper fabricated via nanostructured barium titanate functionalization of wood cellulose fibers. ACS Appl Mater Interfaces 6:7547–7553
42. Alam MM, Mandal D (2016) Native cellulose microfiber-based hybrid piezoelectric generator for mechanical energy harvesting utility. ACS Appl Mater Interfaces 8:1555–1558
43. Zheng Q, Zhang H, Mi H et al (2016) High-performance flexible piezoelectric nanogenerators consisting of porous cellulose nanofibril (CNF)/poly(dimethylsiloxane) (PDMS) aerogel films. Nano Energy 26:504–512
44. Liu Y, Member S, Ren KL, Hofmann HF (2005) Investigation electrostrictive polymers for energy harvesting. IEEE Trans Ultrason Ferroelectr Freq Control 52:2411–2417
45. Guyomar D, Lebrun L, Putson C et al (2009) Electrostrictive energy conversion in polyurethane nanocomposites. J Appl Phys 106:014910
46. Lallart M, Cottinet P-J, Lebrun L et al (2010) Evaluation of energy harvesting performance of electrostrictive polymer and carbon-filled terpolymer composites. J Appl Phys 108:034901
47. Lebrun L, Guyomar D, Guiffard B et al (2009) The characterisation of the harvesting capabilities of an electrostrictive polymer composite. Sens Actuators A Phys 153:251–257
48. Leaver P, Cunningham MJ, Jones BE (1987) Piezoelectric polymer pressure sensors. Sens Actuators 12:225–233
49. Yuan Y, Zhou S, Liu Y, Tang J (2013) Nanostructured macroporous bioanode based on polyaniline-modified natural loofah sponge for high-performance microbial fuel cells. Environ Sci Technol 47:14525–14532
50. Wang Y, Zhang SM, Deng Y et al (2016) Flexible low-grade energy utilization devices based on high-performance thermoelectric polyaniline/tellurium nanorod hybrid films. J Mater Chem A 4:3554–3559
51. Sultana A, Alam MM, Garain S et al (2015) An effective electrical throughput from PANI supplement ZnS nanorods and PDMS-based flexible piezoelectric nanogenerator for power up portable electronic devices: an alternative of MWCNT filler. ACS Appl Mater Interfaces 7:19091–19097
52. Antiohos D, Romano M, Chen J, Razal JM (2013) Carbon nanotubes for energy applications. In: Syntheses and applications of carbon nanotubes and their composites. InTech
53. Romano MS, Gambhir S, Razal JM et al (2012) Novel carbon materials for thermal energy harvesting. J Therm Anal Calorim 109:1229–1235
54. Hu R, Cola BA, Haram N et al (2010) Harvesting waste thermal energy using a carbon-nanotube-based thermo-electrochemical cell. Nano Lett 10:838–846
55. Romano MS, Li N, Antiohos D et al (2013) Carbon nanotube—reduced graphene oxide composites for thermal energy harvesting applications. Adv Mater 25:6602–6606
56. Im H, Kim T, Song H et al (2016) High-efficiency electrochemical thermal energy harvester using carbon nanotube aerogel sheet electrodes. Nat Commun 7:10600
57. Dey A, Bajpai OP, Sikder AK et al (2016) Recent advances in CNT/graphene based thermoelectric polymer nanocomposite: A proficient move towards waste energy harvesting. Renew Sustain Energy Rev 53:653–671

http://www.springer.com/978-3-319-50423-0

Smart Polymer Nanocomposites
Energy Harvesting, Self-Healing and Shape Memory Applications
Ponnamma, D.; Sadasivuni, K.K.; Cabibihan, J.-J.; Al-Maadeed, M.A.A. (Eds.)
2017, XI, 397 p. 183 illus., 131 illus. in color., Hardcover
ISBN: 978-3-319-50423-0